Modeling and Control of High–Voltage Direct–Current Transmission Systems: From Theory to Practice and Back ⋆

Daniele Zonetti [a], Romeo Ortega [a], Abdelkrim Benchaib [b]

[a] *Laboratoire des Signaux et Systèmes, 3, rue Joliot Curie - 91192, Gif-sur-Yvette, France*

[b] *Alstom Grid, 102, avenue de Paris - 91300 Massy, France*

Abstract

The problem of modeling and control of multi–terminal high–voltage direct–current transmission systems is addressed in this paper, which contains four main contributions. First, to propose a unified, physically motivated, modeling framework—based on port–Hamiltonian systems representations—of the various network topologies used in this application. Second, to prove that the system can be globally asymptotically stabilized with a decentralized PI control that exploits its passivity properties. Close connections between the proposed PI and the popular Akagi's PQ instantaneous power method are also established. Third, to reveal the transient performance limitations of the proposed controller that, interestingly, is shown to be intrinsic to PI passivity–based control. Fourth, motivated by the latter, we propose to revisit the so–called primary and secondary control, which is widely used in the power systems community. The performance limitation of the PI, and its drastic improvement using outer–loop controls, are verified via simulations on a three–terminal benchmark example.

Key words: multiterminal HVDC transmission systems; passivity–based control; port–Hamiltonian systems; PI control; primary control; secondary control; performance limitations; nonminimum–phase systems; PQ and DC voltage control; power flow equations.

1 Introduction

We have witnessed in the last few years an ever widespread utilization of renewable energy utilities, mainly based on wind and solar power [18,7]. Because of its intermittent nature the integration of this generating units to the existing alternating–current (AC) distribution network poses a challenging problem [6,24]. For this, and other reasons related to reduced losses and problems with reactive power and voltage stability in AC systems, the option of high–voltage direct–current (HVDC) transmission systems is gaining wide popularity, see [7,22,20] for additional motivations and details.

The main components of an HVDC system are AC to DC power converters, transmission lines and voltage bus capacitors. The power converters connect the AC sources—that are associated to renewable generating units or to AC grids—to an (inductive line–based) HVDC grid through voltage bus capacitors. Two notable features distinguish HVDC systems from standard AC ones: the absence of loads and the central role played by the power converters, whose dynamics is highly *nonlinear*.

For its correct operation HVDC systems—like all electrical power systems—must satisfy a large set of different regulation objectives that are, typically, associated to the multiple time–scale behavior of the system. One way to deal with this issue, that prevails in practice, is the use of hierarchical architectures. These are nested control loops, at different time scales, each one providing references for an inner controller [21,38]. In this paper we are mainly interested in the "innermost" control loop for HVDC transmission systems, that is, the control at the power converter level—in the sequel we will refer to this level as *inner–loop* control. The objective of the inner–loop control is to asymptotically drive the HVDC system towards a desired steady–state regime determined by the user. Regulation should be achieved selecting a suitable switching policy for the converters. A major practical constraint is that the control should be *decentralized*. That is, the controller of each power converter has only available for measurement its corre-

⋆ Corresponding author D. Zonetti. Tel. +33 1 69 85 17 12.
Email addresses: daniele.zonetti@lss.supelec.fr (Daniele Zonetti), romeo.ortega@lss.supelec.fr (Romeo Ortega), abdelkrim.benchaib@alstom.com (Abdelkrim Benchaib).

sponding coordinates, with no exchange of information between them.

Starting from single AC/DC converter models many strategies have been proposed for the inner–loop control of the power converters used in HVDC systems [2,23,26], with the dominating structure consisting of nested PI loops: an inner current control loop and an outer loop to regulate the capacitors voltage. The rationale used to justify this structure is the time–scale separation between currents and voltages. However, with the notable exception of [34], the performance claims are not corroborated by rigorous stability proofs. Because of the absence of theoretical analysis, a time–consuming and expensive procedure to tune the gains of the PIs is then required to complete the design. This is typically done based on the linearization of the system that, because of the highly nonlinear behavior of the converters and the wide range of the operating regimes, often yields below–par performances.

The main objective of this paper is to contribute, if modestly, towards the development of a general, theoretically–founded procedure for the modeling, analysis and control of HVDC systems. With the intention to bridge the gap between theory and applications, one of our main concerns is to establish connections between existing engineering solutions, usually derived via *ad–hoc* considerations, and the solutions stemming from theoretical analysis. In particular, it is shown that modifying the theoretically–based inner–loop controller to incorporate the standard considerations of outer–loop control considerably improves its transient performance.

The contributions of the paper are the following.

(C1) To propose a unified, physically motivated, modeling framework of the various network topologies used in HVDC systems. This framework is based on port–Hamiltonian (pH) models of the system components [10,35,39] combined with a suitable graph theoretic representation of their interconnection [11]. The lines are modeled as simple series resistance–inductance (RL) circuits and the capacitors are assumed to be leaky elements, all components being linear. Although many different kinds of power converters are used in applications the dominant structure is the so–called voltage–source rectifier (VSR), which are the ones considered in the paper. The network is described via a *meshed topology*, which allows for possible direct connection of the VSRs with the transmission lines.

(C2) In the spirit of [16,19,29] we show that the incremental model of the VSR defines a *passive* map with respect to some suitably designed output. A consequence of this fundamental property is that a decentralized PI passivity–based controller (PBC) *globally asymptotically stabilizes* any assignable equilibrium, with no restriction imposed on the (positive) gains of the PI–PBC. It is also shown that the proposed PI–PBC is closely related with Akagi's PQ instantaneous power method [2] that was derived (without a stability analysis) invoking power balance considerations and is a standard in applications.

(C3) It is well–known that passive systems are minimum phase and have relative degree one [5,35]. Consequently, the attainable performance of a PI–PBC is limited by its associated zero dynamics. Another contribution of the paper is the proof that, in HVDC systems, the zero dynamics is "extremely slow", stymying the achievement of fast transient responses. On the other hand, it is also shown that other inner–loop PI controllers reported in the literature may exhibit unstable behavior because the zero dynamics associated to the corresponding outputs are *non–minimum phase*.

(C4) To overcome the aforementioned limitation we propose to revisit the so–called *primary* control [31,3], widely used in the power systems community. The primary control is an outer–loop that generate the references for the inner–loop control. Although only a local stability analysis is carried–out, the transient performance limitation of the PI–PBC, and its drastic improvement using primary control, are verified via simulations on a threee-terminals benchmark example.

(C5) Our final contribution relates to the design of the last outer–loop controller, usually called *secondary control* [15,31,1]. Although there is no universal agreement to define the tasks of this control loop it usually relates to the regulation of the flow of active and reactive power to be injected into the network while keeping the voltage of the capacitors near a desired constant value. Most popular approaches, which usually invoke *ad–hoc* considerations, are reviewed and contextualized in the present framework.

The remaining part of the paper is structured as follows. In Section 2, the mathematical model of the system is established (C1). Then, to determine the achievable behaviors, a study of the assignable equilibria is necessary. This analysis is done in Section 3. Our main contribution (C2) is next developed in Section 4, with the design of the decentralized passivity–based PI controller. Slow transients exhibited in simulations motivate the subsequent performance analysis (C3), that is carried–out in Section 5. Sections 6 and 7 are then devoted to revisit standard primary (C4) and secondary controllers (C5). We wrap–up the paper with conclusions and future work in Section 8.

Notation All vectors are column vectors. Given positive integers n, m we use $\underline{0}_n \in \mathbb{R}^n$ to denote the vector of all zeros, $\mathbb{1}_n \in \mathbb{R}^n$ the vector with all ones, $\mathbb{I}_n$ the $n \times n$ identity matrix, $\underline{0}_{n\times m}$ the $n \times m$ column matrix of all zeros. $x := \text{col}(x_1, \dots, x_n) \in \mathbb{R}^n$ denotes a vector with entries $x_i \in \mathbb{R}$, when clear from the context we simply write $x := \text{col}(x_i)$. $\text{diag}\{a_i\}$ is a diagonal matrix

with entries $a_i \in \mathbb{R}$ and bdiag$\{A_i\}$ denotes a block diagonal matrix with entries the matrices A_i. For a function $f : \mathbb{R}^n \to \mathbb{R}$, ∇f denotes the transpose of its gradient. The subindex i, preceded by a comma when necessary, denotes elements corresponding to the i-th subsystem. To deal with bilinear representations we further use a by-blocks adaptation of the Kronecker product, that we represent with the symbol $\otimes$, and define as follows. Let $A \in \mathbb{R}^{mn\times mn}$ a square matrix constituted by n^2 square blocks of dimension m, denoted as $A_{ij} \in \mathbb{R}^{m\times m}$, and $B \in \mathbb{R}^m$. Then

$$A = \begin{bmatrix} A_{11} & \dots & A_{1m} \\ \vdots & \ddots & \vdots \\ A_{m1} & \dots & A_{mm} \end{bmatrix} \quad \Rightarrow \quad A \otimes B := \begin{bmatrix} A_{11}B & \dots & A_{1m}B \\ \vdots & \ddots & \vdots \\ A_{m1}B & \dots & A_{mm}B \end{bmatrix}.$$

2 Energy–based Modeling

In [11] it was shown that electrical power systems can be represented by a directed graph [1] where the relevant electrical components correspond to edges and the buses correspond to nodes. Moreover, to underscore the physical structure of the components, they are modeled as pH systems. In this section we apply the same procedure to describe the dynamics of HVDC transmission systems.

2.1 Assumptions

As indicated in the Introduction, in HVDC transmission systems no loads exist and the relevant components are: VSRs, *RL* transmission lines and voltage bus capacitors. Throughout the paper we make the following assumptions, which are widely accepted in practice.

(A1) Balanced operation of the three phase line voltages.
(A2) Synchronized operation of the VSRs.
(A3) Ideal four quadrant operation of the VSRs.

Assumptions A1 and A2 considerably simplify the modeling and control problems, as they allow the description of the three–phase dynamics of the VSRs in suitably oriented *dq*0 reference frames, where the value of the *zero*–component is always zero, thus reducing the three AC quantities to two DC quantities. This allows us to express the regulation objective as a standard *equilibrium stabilization* problem of the nonlinear dynamical system describing the behavior of the HVDC system. Assumption A3 directly follows by assuming HVDC transmission system based on VSRs instead of current source rectifiers, which is an alternative converter topology used in HVDC systems. As a matter of fact, since the VSRs do not depend on line–commutations, all the four quadrants of the operating plane are possible, hence Assumption A3 is automatically satisfied for the system under consideration [1].

Remark 2.1 Synchronized operation of the VSRs is usually achieved via robust phase–locked–loop detection of the latching frequencies [38].

2.2 Network topologies: A graph description

We can mainly distinguish two kinds of topologies used in HVDC transmission systems: *radial* and *meshed* topology [12,4,14], which are illustrated in Fig. 1. The radial topology is widely used for systems in which a certain number of off–shore stations feeds on–shore stations with no connection between them. This is the case for example of on–shore stations situated on opposite seacoasts while the off–shore stations are placed in their middle [4,22]. Though there exist a great variety of cases in which a radial topology correctly describes the structure of the network, in a more general setting we have to consider the situation in which the stations are directly connected with lines, called meshed topology. In the interest of brevity, we present here a systematic way to build global pH models only for the meshed topology. For a radial topology, analogous results can be obtained, for which the interested reader is referred to [40].

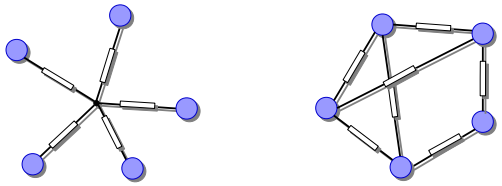

Fig. 1. Nodal representation of HVDC transmission systems with radial and meshed topologies.

In order to give a formal representation of a topology we adopt the following definitions. We call a bus a *VSR-bus* if a VSR is connected to it and we call a bus a *capacitor-bus* when only a capacitor is connected to it. Furthermore, we call a bus a *reference-bus* when all the voltages of the buses in the network are measured with respect to it. As the reference-bus is assumed to be at ground potential, is also denoted as *ground*. A general topology is then described by the incidence matrix M associated to the graph, where the nodes represent the ground, the VSR and the capacitor-buses; the edges represent the VSRs, the lines and the single capacitors that are interconnected to the ground or to the voltage buses.

In a meshed topology each VSR is connected to the ground and to a VSR–bus, while the lines directly connect VSR–buses, according to a determined meshed

[1] A directed graph is an ordered 3-tuple, $\mathcal{G} = \{\mathcal{V}, \mathcal{E}, \Pi\}$, consisting of a finite set of nodes $\mathcal{V}$, a finite set of directed edges $\mathcal{E}$ and a mapping Π from $\mathcal{E}$ to the set of ordered pairs of $\mathcal{V}$, where no self-loops are allowed.

structure. The number n of VSRs is the same of voltage buses, ground excluded, and is lower or equal to the number ℓ of lines. Formally this can be represented by a graph $\mathcal{G} := \{\mathcal{V}, \mathcal{E}, \Pi\}$ constituted by: $n+1$ ordered nodes, where n nodes are associated to the VSR–buses and one node to the ground; $n+\ell$ ordered edges, where n edges are associated to the VSRs and ℓ edges to the lines. The incidence matrix then, following the mentioned order, takes the form

$$M = \begin{bmatrix} \mathbb{I}_n & M_1 \\ -\mathbb{1}_n^\top & 0_\ell^\top \end{bmatrix} \in \mathbb{R}^{(n+1)\times(n+\ell)}, \qquad (2.1)$$

where M_1 is the incidence matrix of the subgraph obtained eliminating the VSRs edges and the ground node.

Remark 2.2 In a meshed topology the only relevant components are the VSRs and the RL transmission lines. As a matter of fact, because a VSR is associated to each node, the voltage bus capacitors can be represented by an equivalent VSR output capacitor, that results to be the parallel interconnection of all capacitors attached to the node.

2.3 Port–Hamiltonian models of the elements

As explained above the edges of the graph $\mathcal{G}$ contain the electrical components of the HVDC system, namely n VSRs and ℓ RL transmission lines, while the nodes are the buses. In this section we derive a pH representation of these elements, which are then interconnected—through power preserving interconnections—via the graph. Besides its physically appealing nature, the choice of a pH model is motivated by the fact that—similarly to [16]—this structure is instrumental to derive the passivity property exploited in the controller design. To enhance readability the models of the VSRs and the transmission lines are presented separately.

2.3.1 Voltage source rectifiers

In [10,16,40] the well–known average model of a single VSR shown in Fig. 2, expressed in dq–coordinates and written in (perturbed) pH form is given. Similarly, a *set* of n VSRs can also be represented in pH form as

$$\begin{aligned} \dot{x}_R &= [\mathcal{J}_R(u) - \mathcal{R}_R]\nabla\mathcal{H}_R + E_1 V - E_3 i_R \\ v_R &= E_3^\top \nabla\mathcal{H}_R, \end{aligned} \qquad (2.2)$$

where we use the following definitions.

- State space variables the collection of inductors fluxes $(\phi_{d,i}, \phi_{q,i})$ and capacitor charges $q_{c,i}$ of every VSR, that is, $x_R := \text{col}(\text{col}(\phi_{d,i}), \text{col}(\phi_{q,i}), \text{col}(q_{c,i})) \in \mathbb{R}^{3n}$.
- Energy function $\mathcal{H}_R(x_R) := \frac{1}{2} x_R^\top Q_R x_R$, with [2]

$$L_R := \text{diag}\{L_{r,i}\}, \quad C_R := \text{diag}\{C_{r,i}\}$$

and

$$Q_R := \text{bdiag}\{L_R^{-1}, L_R^{-1}, C_R^{-1}\},$$

where $L_{r,i}, C_{r,i}$ are the inductance and capacitance of each VSR, respectively.
- Duty cycles $u := \text{col}(u_{Rd}, u_{Rq}) \in \mathbb{R}^{2n}$, where $u_{Rd} := \text{col}(u_{d,i})$ and $u_{Rq} := \text{col}(u_{q,i})$.
- External voltage sources $V := \text{col}(v_{d,i}) \in \mathbb{R}^n$, where $v_{d,i}$ is the d component of the AC sources. These voltages are assumed constant and positive.
- Port variables the out–going currents $i_R := \text{col}(i_{dc,i}) \in \mathbb{R}^n$ and the voltages $v_R := \text{col}(v_{dc,i}) \in \mathbb{R}^n$.
- Interconnection matrix

$$\mathcal{J}_R(u) := \mathcal{J}_{R0} \otimes \Omega + \mathcal{J}_{Rd} \otimes u_{Rd} + \mathcal{J}_{Rq} \otimes u_{Rq} \quad (2.3)$$

where

$$\mathcal{J}_{R0} := \begin{bmatrix} 0 & L_R & 0 \\ -L_R & 0 & 0 \\ 0 & 0 & 0 \end{bmatrix}, \mathcal{J}_{Rd} := \begin{bmatrix} 0 & 0 & -\mathbb{I}_n \\ 0 & 0 & 0 \\ \mathbb{I}_n & 0 & 0 \end{bmatrix}, \mathcal{J}_{Rq} := \begin{bmatrix} 0 & 0 & 0 \\ 0 & 0 & -\mathbb{I}_n \\ 0 & \mathbb{I}_n & 0 \end{bmatrix},$$

with $\Omega := \text{col}(\omega_i)$ the AC sides frequencies.
- Dissipation matrix $\mathcal{R}_R := \text{bdiag}\{R_R^{-1}, R_R^{-1}, G_R^{-1}\}$, where $R_R := \text{diag}\{R_{r,i}\}$ and $G_R := \text{diag}\{G_{r,i}\}$, with $R_{r,i}, G_{r,i}$ the resistance and conductance of each VSR.
- Port matrices $E_1 := \begin{bmatrix} \mathbb{I}_n & 0 & 0 \end{bmatrix}^\top$, $E_3 := \begin{bmatrix} 0 & 0 & \mathbb{I}_n \end{bmatrix}^\top \in \mathbb{R}^{3n\times n}$.

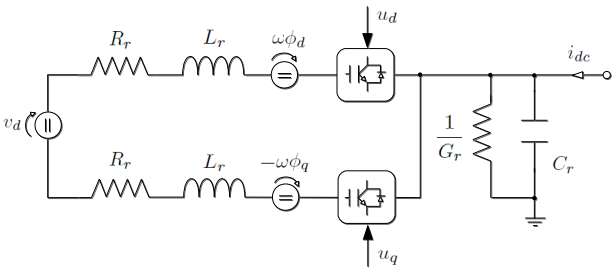

Fig. 2. Schematic diagram of the equivalent circuit of a VSR in dq frame.

Remark 2.3 Notice that, in view of the skew–symmetry of $\mathcal{J}_R(u)$, the VSRs satisfy the power balance

[2] Unless indicated otherwise all physical parameters of the system are positive constants.

equation

$$\underbrace{\dot{\mathcal{H}}_R}_{\text{stored power}} = -\underbrace{x_R^\top Q_R \mathcal{R}_R Q_R x_R}_{\text{dissipated power}} + \underbrace{x_R^\top Q_R E_1 V - x_R^\top Q_R E_3 i_R}_{\text{supplied power}} \tag{2.4}$$

2.3.2 Transmission lines

A set of ℓ RL transmission lines can be represented by the pH system

$$\begin{aligned} \dot{x}_L &= -\mathcal{R}_L \nabla \mathcal{H}_L + v_L \\ i_L &= -\nabla \mathcal{H}_L, \end{aligned} \tag{2.5}$$

with the following definitions.

- State space variables the collection of inductor fluxes $x_L := \text{col}(\phi_{\ell,i}) \in \mathbb{R}^\ell$ of every line.
- Energy function

$$\mathcal{H}_L(x_L) := \frac{1}{2} x_L^\top Q_L x_L, \qquad Q_L := \text{diag}\{\frac{1}{L_{\ell,i}}\},$$

  where $L_{\ell,i}$ is the inductance of the line.
- Port variables the voltages at the terminals $v_L := col(v_{L,i}) \in \mathbb{R}^\ell$ and the inductors currents $i_L := \text{col}(i_{\ell,i}) \in \mathbb{R}^\ell$.
- Dissipation $\mathcal{R}_L = \text{diag}\{R_{\ell,i}\}$, with $R_{\ell,i}$ the resistance of the line.

2.4 Overall interconnected system

The interconnection laws can be obtained following the approach used in [36], where the Kirchhoff's current and voltage laws (KCL and KVL, respectively) are expressed in relation to the incidence matrix. For a *meshed* topology we have then

$$\begin{aligned} &\textsf{[KCL]} \qquad M\mathcal{I}_e = \underline{0}_{n+1} \\ &\textsf{[KVL]} \qquad M^\top \mathcal{V} = \mathcal{V}_e, \end{aligned} \tag{2.6}$$

where $\mathcal{I}_e := \text{col}(i_R, i_L)$, $\mathcal{V}_e := \text{col}(v_R, v_L)$ and $\mathcal{V} := \text{col}(v_1, \dots, v_n)$, v_0 are the edge currents, the edge voltages, the nodes potentials and the ground potential, respectively. The ground potential $v_0 = 0$ by definition. From (2.6) and (2.1) then follows

$$\begin{aligned} i_R + M_1 i_L = \underline{0}_n, \quad -\mathbb{1}_n^\top i_R = 0, \\ v = v_R, \quad M_1^\top v = v_L. \end{aligned} \tag{2.7}$$

Recalling the expression for i_L from (2.2) and v_R from (2.5) we have

$$i_R = M_1 \nabla \mathcal{H}_L, \qquad v_L = M_1^\top E_3^\top \nabla \mathcal{H}_R. \tag{2.8}$$

To obtain the overall pH representation it is sufficient to combine (2.2), (2.5) and (2.8), thus leading to:

$$\dot{x} = [\mathcal{J}(u) - \mathcal{R}] \nabla \mathcal{H} + EV, \tag{2.9}$$

with the following definitions.

- State space variables $x := \text{col}(x_R, x_L) \in \mathbb{R}^{3n+\ell}$.
- Energy function $\mathcal{H}(x) := \mathcal{H}_R(x) + \mathcal{H}_L(x)$.
- Duty cycles (controls) $u := \text{col}(u_{Rd}, u_{Rq}) \in \mathbb{R}^{2n}$.
- Interconnection matrix

$$\mathcal{J}(u) := \mathcal{J}_0 + \mathcal{J}_d \otimes u_{Rd} + \mathcal{J}_q \otimes u_{Rq} \tag{2.10}$$

  with the following definitions:

$$\mathcal{J}_0 := \begin{bmatrix} J_{R0} \otimes \Omega & -E_3 M_1 \\ M_1^\top E_3^\top & \underline{0}_{\ell \times \ell} \end{bmatrix}, \; \begin{aligned} \mathcal{J}_d &:= \text{bdiag}\{J_{Rd}, \underline{0}_{\ell \times \ell}\}, \\ \mathcal{J}_q &:= \text{bdiag}\{J_{Rq}, \underline{0}_{\ell \times \ell}\}. \end{aligned}$$

- Dissipation matrix

$$\mathcal{R} := \text{bdiag}\{\mathcal{R}_R, \mathcal{R}_L\} > 0. \tag{2.11}$$

- Input matrix $E := \left[\begin{smallmatrix} E_1^\top & \underline{0}_{\ell \times n}^\top \end{smallmatrix} \right]^\top$.

Remark 2.4 To simplify the notation in the pH representation we have selected a state representation of the system using energy variables, that is, inductor fluxes and capacitor charges, instead of the more commonly used co–energy variables, *i.e.*, inductor currents and capacitor voltages. See (4.7) and [25] for the derivation of the pH model in the latter coordinates. We recall that they are related by

$$i_d = \frac{\phi_d}{L}, \quad i_q = \frac{\phi_q}{L}, \quad v_C = \frac{q_C}{C}, \quad i_L = \frac{\phi_L}{L_\ell}. \tag{2.12}$$

Remark 2.5 For ease of presentation we have assumed that the state of the system lives in $\mathbb{R}^{3n+\ell}$. Due to physical and technological constraints it is actually only defined in a subset of $\mathbb{R}^{3n+\ell}$. In particular, the voltage of the DC link v_C is strictly bounded away from zero.

3 Assignable Equilibria

A first step towards the development of a control strategy for the system (2.9) is the definition of its achievable, steady–state behavior, which is determined by the assignable equilibria. That is, the (constant) vectors $x^\star \in \mathbb{R}^{3n+\ell}$ such that

$$[\mathcal{J}(u^\star) - \mathcal{R}] \nabla \mathcal{H}(x^\star) + GV = \underline{0}_{3n+\ell}$$

for some (constant) vector $u^\star \in \mathbb{R}^{2n}$. To identify this set we establish the following lemmata.

Lemma 3.1 The equilibria of the transmission line coordinates are given by

$$x_L^\star = (\mathcal{R}_L Q_L)^{-1} M_1^\top E_3^\top Q_R x_R^\star. \tag{3.1}$$

PROOF. Setting to to zero the left–hand side of (2.5), calculated at $x_L^\star$, gives

$$\underline{0}_\ell = -\mathcal{R}_L Q_L x_L^\star + v_L^\star \quad \Rightarrow \quad x_L^\star = (\mathcal{R}_L Q_L)^{-1} v_L^\star.$$

Moreover, from (2.8) we have $v_L^\star = M_1^\top E_3^\top Q_R x_R^\star$, that replaced in the equation above completes the proof.

Lemma 3.2 The equilibria of the VSRs coordinates are the solution of the quadratic equation

$$x_R^{*\top} Q_R (\mathcal{R}_R + E_3 M_1 \mathcal{R}_L^{-1} M_1^\top E_3^\top) Q_R x_R^\star + x_R^{*\top} Q_R E_3 V = \underline{0}_n. \tag{3.2}$$

PROOF. In [28] it is shown that the equilibrium of a VSR is obtained by setting equal to zero the power balance equation (2.4), that for a set of n VSR is equivalent to set

$$-x_R^{*\top} Q_R x_R^\star + x_R^{*\top} Q_R E_1 V - x_R^{*\top} Q_R E_3 i_R^\star = \underline{0}_n.$$

Recalling now (2.8) we have $i_R^\star = M_1 Q_L x_L^\star$ and we can use (3.1) to obtain (3.2), completing the proof.

We are now ready to present the main result of the section, whose proof follows immediately from the lemmata above.

Proposition 3.3 The set of assignable equilibria of the system (2.9) is given by

$$\mathcal{E} := \{x^\star \in \mathbb{R}^{3n+\ell} \mid (3.1) \text{ and } (3.2) \text{ hold}\}. \tag{3.3}$$

From the derivations above it is clear that the equilibria of the network are univocally determined by the equilibria of the VSRs. Moreover, the latter should satisfy the quadratic equations (3.2), which are the well–known *power flow steady–state equations* (PFSSE) of the system. A question of interest is how to select from this set the equilibrium points that correspond to some *desired behavior*. In the latter definition there are many practical considerations to be taken into account, therefore we do not dwell any longer on this issue at this point, and postpone this discussion to Sections 6 and 7.

Remark 3.4 It is well–known that for affine systems of the form $\dot{x} = f(x) + g(x)u$ the assignable equilibrium set is given by

$$\{x^\star \in \mathbb{R}^n \mid g^\perp(x^\star) f(x^\star) = 0\}$$

where $g^\perp(x)$ is a full–rank left annihilator of $g(x)$. Moreover, given $x^\star$, the corresponding equilibrium control $u^\star$ is *univocally* determined by

$$u^\star = -\left[(g^\top g)^{-1} g^\top f\right](x^\star).$$

Since (2.9) is clearly of this form this relations hold true for the HVDC system under study. See [28] for additional details on this issue.

4 Main Result: Inner Loop Control

As indicated in the introduction in this paper we are mainly interested in the inner–loop control of HVDC transmission systems, that is, the control at the VSR level. For this problem we present in this section a decentralized, globally asymptotically stabilizing, PI–PBC for the HVDC transmission system (2.9). The construction of the controller is inspired by our previous works on PI–PBC reported in [16] and [19], which exploit the property of passivity of the *incremental model*. The interested reader is referred to these references for additional details.

As indicated above, it is assumed that a desired operating point $x^\star \in \mathcal{E}$ has already been selected—further discussions on its choice are deferred to Sections 6 and 7. To place the proposed PI–PBC in context, in the last part of this section we briefly review the most commonly used inner–loop controls for HVDC transmission systems and establish the connection with the widely popular Akagi's PQ method.

4.1 Passivity of the incremental model

Along the lines of Proposition 1 in [16], it is possible to establish passivity of the incremental model of the global HVDC transmission system (2.9) with respect to a suitable defined output. As is well–known, global regulation of a passive output can be achieved with a simple PI controller. Regulation of the state to the desired equilibrium then follows provided a suitable detectability assumption is satisfied [35].

Proposition 4.1 Consider the HVDC transmission system (2.9). Let $x^\star \in \mathcal{E}$ be the desired equilibrium with corresponding (univocally defined) control $u^\star \in \mathbb{R}^{2n}$. Define the error signals

$$\tilde{x} = x - x^\star, \quad \tilde{u} = u - u^\star \tag{4.1}$$

and the output signal

$$y = \begin{bmatrix} x_R^{*\top} Q_R \mathcal{J}_{Rd} Q_R x_R \\ x_R^{*\top} Q_R \mathcal{J}_{Rq} Q_R x_R \end{bmatrix} \in \mathbb{R}^{2n}. \tag{4.2}$$

The mapping $\tilde{u} \to y$ is *passive*. More precisely, the system verifies the dissipation inequality

$$\dot{\mathcal{H}}_d \leq y^\top \tilde{u}, \tag{4.3}$$

with storage function

$$\mathcal{H}_d(\tilde{x}) = \frac{1}{2}\tilde{x}^\top Q \tilde{x}.$$

PROOF. The proof mimics the proof of Proposition 1 in [16]. We first notice that

$$\mathcal{J}(u) = \mathcal{J}_0 + g(x) \otimes u,$$

where we defined

$$g(x) := \Big[\mathcal{J}_d Q x \;\; \mathcal{J}_q Q x.\Big]$$

Hence, it is possible to write (2.9) in the alternative form

$$\begin{aligned} \dot{x} &= (\mathcal{J}_0 - \mathcal{R})Qx + EV + g(x) \otimes u \\ &= (\mathcal{J}_0 - \mathcal{R})Q(\tilde{x} + x^\star) + EV + g(x) \otimes (\tilde{u} + u^\star) \\ &= (\mathcal{J}_0 - \mathcal{R})Q\tilde{x} + g(x) \otimes \tilde{u} + g(\tilde{x}) \otimes u^\star \end{aligned} \tag{4.4}$$

where we have used (4.1) to get the second equation and the fact that the assignable equilibria $x^\star$ and corresponding (constant) control $u^\star$ satisfy

$$(\mathcal{J}_0 - \mathcal{R})Qx^\star + EV + g(x^\star) \otimes u^\star = 0,$$

to obtain the third equation.

The derivative of $\mathcal{H}_d$ along the trajectories of the incremental model (4.4) yields

$$\begin{aligned} \dot{\mathcal{H}}_d &= -\tilde{x}^\top Q\mathcal{R}Q\tilde{x} + \tilde{x}^\top Q g(x) \otimes \tilde{u} \\ &= -\tilde{x}^\top Q\mathcal{R}Q\tilde{x} + y^\top \tilde{u} \end{aligned}$$

where skew–symmetry of $\mathcal{J}_0$, $\mathcal{J}_d$ and $\mathcal{J}_q$ is used in the first equation, and the fact that the output signal (4.2) can be rewritten as

$$y = g^\top(x^\star)Qx = g^\top(x^\star)Q\tilde{x}$$

to obtain the second identity. The proof is completed recalling that the dissipation matrix verifies $\mathcal{R} > 0$ to get the bound (4.3).

4.2 PI passivity–based control

We are in position to present the first main result of the paper.

Proposition 4.2 Consider the HVDC transmission system (2.9), with a desired steady–state $x^\star \in \mathcal{E}$, in closed–loop with the decentralized PI control

$$\begin{aligned} \dot{\zeta} &= y \\ u &= -K_P y - K_I \zeta \end{aligned} \tag{4.5}$$

with y given in (4.2) and gain matrices

$$\begin{aligned} K_P &= \text{bdiag}\{k_{P,i}\} \in \mathbb{R}^{2n \times 2n} \\ K_I &= \text{bdiag}\{k_{I,i}\} \in \mathbb{R}^{2n \times 2n}, \end{aligned} \tag{4.6}$$

with $k_{P,i}, k_{I,i} \in \mathbb{R}^{2\times 2}$ *arbitrary* positive definite matrices. The equilibrium point $(x^\star, K_I^{-1}u^\star)$ is globally asymptotically stable (GAS).

PROOF. Define the Lyapunov function candidate

$$W(\tilde{x}, \tilde{\zeta}) := \mathcal{H}_d(\tilde{x}) + \frac{1}{2}\tilde{\zeta}^\top K_I \tilde{\zeta},$$

where

$$\tilde{\zeta} := \zeta - K_I^{-1}u^\star.$$

The derivative of $W(x, \zeta)$ along the trajectories of the closed–loop system (4.4), (4.5) is given by

$$\begin{aligned} \dot{W} &= -\tilde{x}^\top Q\mathcal{R}Q\tilde{x} + y^\top \tilde{u} + \tilde{\zeta}^\top K_I y \\ &= -\tilde{x}^\top Q\mathcal{R}Q\tilde{x} + y^\top \tilde{u} - y^\top(K_P y + \tilde{u}) \\ &= -\tilde{x}^\top Q\mathcal{R}Q\tilde{x} - y^\top K_P y \leq 0 \end{aligned}$$

that proves global stability. Asymptotic stability follows, as done in [16], using LaSalle's arguments. Indeed, from the inequality above and the definition of $\mathcal{R}$ in (2.11) it is clear that all components of the error state vector $\tilde{x}$ tend to zero.

Remark 4.3 The proposed PI–PBC is decentralized in the sense that, for its implementation, each VSR control requires only the measurement of its corresponding inductor currents and capacitor voltage. Guaranteeing this property motivates our choice of block diagonal gain matrices (4.6).

Remark 4.4 The PI–PBC requires the selection of the desired values for the inductor currents and capacitor voltages that, clearly, cannot all be chosen arbitrarily. Instead, they have to be selected from the set of assignable equilibrium points $\mathcal{E}$, that is determined by the PFSSE. This set has a rather simple structure: the quadratic

equation (3.2) defines the VSRs variables from which we *univocally* determine the transmission lines coordinates via (3.1).

4.3 Other inner–loop controllers reported in the literature

In this section we review some of the inner–loop controllers for VSRs reported in the literature. The vast majority of the papers reported on this topic—and, in general, of control of power converters [21,26]—uses the description of the dynamics in co–energy variables. To facilitate the reference to these works, to some of which we refer here, we give now this model that is immediately obtained from (2.2) and (2.12) as [3]

$$\begin{aligned} L\dot{i}_d &= -Ri_d + L\omega i_q - v_C u_d + v_d \\ L\dot{i}_q &= -L\omega i_d - Ri_q - v_C u_q \\ C\dot{v}_C &= i_d u_d + i_q u_q - Gv_C - i_{dc}. \end{aligned} \tag{4.7}$$

The total energy of the VSR is

$$\mathcal{H}(i_d, i_q, v_C) := \frac{1}{2}\left(Li_d^2 + Li_q^2 + Cv_C^2\right),$$

and the power balance is

$$\dot{\mathcal{H}} = -R(i_d^2 + i_q^2) - Gv_C^2 + P - P_{dc}, \tag{4.8}$$

where we have defined the active and DC powers

$$P = v_d i_d, \qquad P_{dc} = v_C i_{dc}. \tag{4.9}$$

It is also common to define the reactive power as $Q = v_d i_q$.

A caveat regarding the subsequent analysis is, however, necessary. When the VSRs are connected to the transmission lines the currents i_{dc} are linked to the currents on the line via (2.7), which are clearly nonconstant. However, to simplify the analysis, we exploit the fact that their rate of change is slow (with respect to the VSR dynamics) and assume that they are *constant*. Under this assumption the assignable equilibrium set of (4.7) is given as

$$\mathcal{E} = \{x \in \mathbb{R}^3 \mid R(i_d^2 + i_q^2) - v_d i_d + Gv_C^2 + i_{dc} v_C = 0\}. \tag{4.10}$$

Since v_d and i_{dc} are constant, it is then clear that the regulation of P, Q and P_{dc} are equivalent to the regulation of i_d, i_q and v_C, respectively. In practice, because of the small losses of the VSR, the value of P slightly differs from P_{dc}, and consequently there is no interest in regulating the pair i_d and v_C at the same time.

In the literature it is then common to distinguish two modes of operation for a VSR:

- *PQ control mode*, when the VSR is required to control the active and reactive power. This is achieved regulating to zero the output

$$y_I = \begin{bmatrix} i_d - i_d^{\text{ref}} \\ i_q - i_q^{\text{ref}} \end{bmatrix}, \tag{4.11}$$

  where the superscript $(\cdot)^{\text{ref}}$ is used to denote reference values—that *do not* necessarily belong to the assignable equilibrium set. These kind of schemes are also called *direct current control* [32].
- *DC voltage control mode*, when the VSR is required to control reactive power and DC voltage. In this case, the regulated output is

$$y_V = \begin{bmatrix} v_C - v_C^{\text{ref}} \\ i_q - i_q^{\text{ref}} \end{bmatrix}. \tag{4.12}$$

  These kind of schemes are also called *direct output voltage control* [32].

To regulate the outputs (4.11) and (4.12) different controllers have been proposed in the literature, ranging from simple PI control [23,26] to feedback linearization [8,9,33]. Some of these papers include some (invariably local) stability analysis. In Section 5 we prove that y_I and y_V, used for the PI's or with respect to which feedback linearization is performed, have *unstable zero dynamics*. Consequently, applying high gains in the PIs will induce instability and the internal behavior of the feedback linearizing schemes will be unstable. [4] Simulations in Subsection 5.4 show that instability indeed arises for these schemes.

For the sake of comparison we write now the passive output (4.2) in co–energy variables for a single VSR as

$$y = \begin{bmatrix} v_C^\star i_d - i_d^\star v_C \\ v_C^\star i_q - i_q^\star v_C \end{bmatrix}, \tag{4.13}$$

where we recall that $(i_d^\star, i_q^\star, v_C^\star) \in \mathcal{E}$, that is, they belong to the assignable equilibrium set.

Remark 4.5 The PI–PBC is *universal*, in the sense that it can operate either in *PQ* or *DC voltage control*

[3] For ease of presentation we restrict the discussion here to a *single* VSR. The extension to multiple VSRs being straightforward.

[4] This well–known phenomenon of nonlinear systems [17] is akin to cancellation of unstable zeros of the plant with the unstable poles of the controller in linear systems.

mode, depending on which equilibria are assigned as desired references, and which one is consequently determined via the PFSSE. One important advantage of this universal feature is that there is *no need to switch* between different controllers when the VSRs are requested to change their mode of operation—this is in contrast with other inner–loop schemes that require switchings between controllers, which is clearly undesirable in practice.

4.4 Relation of PI–PBC with Akagi's PQ method

A dominant approach for the design of controllers for reactive power compensation using active filters (for three–phase circuits) is the PQ instantaneous power method proposed by Akagi, *et al.* in [2]. It consists in an outer–loop that generates references for the inner PI loops. The references are selected in order to satisfy a very simple heuristic: the AC active power P has to be equal to the DC power P_{dc}, thus ensuring the maximal power transfer from AC to DC side, and the reactive power should take a desired value.

Now, using (4.9) define the active AC and DC powers at the equilibrium as

$$P^\star = v_d i_d^\star, \quad P_{dc}^\star = v_C^\star i_{dc}.$$

Consider then the following equivalences

$$\begin{aligned} P^\star P_{dc} = P_{dc}^\star P &\Leftrightarrow v_C^\star i_d = i_d^\star v_C \\ &\Leftrightarrow y_1 = 0, \end{aligned}$$

with y_1 the first component of the passive output (4.13). Similarly, for the reactive power

$$\begin{aligned} Q^\star P_{dc} = P_{dc}^\star Q &\Leftrightarrow v_C^\star i_q = i_q^\star v_C \\ &\Leftrightarrow y_2 = 0, \end{aligned}$$

with y_2 the second component of the passive output (4.13). In other words, the objective of the PI–PBC to drive the passive output y to zero can be reinterpreted as a power equalization objective identical to the one used in Akagi's PQ method.

5 Performance Limitations of Inner–Loop PIs

Quality assessment of control algorithms is a difficult task—epitomized by the classical performance versus robustness tradeoff, neatly captured by the stability margins in linear designs. The situation for nonlinear systems, where the notions of (dominant) poles and frequency response are specious, is far more complicated. In any case, it is well–known that the achievable performance in control systems is limited by the presence of minimum phase zeros [13,27,30].

In this section an attempt is made to evaluate the performance limitations of the inner–loop PI controllers discussed in the previous section. Towards this end, we compute the zero dynamics of the VSR system (4.7) for the outputs y (4.2), y_I (4.11) and y_V (4.12). All three outputs have relative degrees $\{1, 1\}$, hence their zero dynamics is of order one but, while it is exponentially stable for the passive output y it turns out that—for normal operating regimes of the VSR—it is *unstable* for y_I and y_V. If the zero dynamics is *unstable* cranking up the controller gains yields an unstable behavior. This should be contrasted with the passive output y that, as shown in Proposition 4.2 yields an asymptotically stable closed–loop system for all positive gains. [5]

To simplify the derivations we consider only the case of $i_q^\star = 0$. This assumption is justified since it corresponds to fixing to zero the desired value of the reactive power, which is a common operating mode of VSRs. Moreover, this is done without loss of generality because it is possible to show—alas, with messier calculations—that the stability of the zero dynamics is the same for the case of $i_q^\star \neq 0$, which may arise when the VSR is associated to an AC grid and not to a renewable energy source.

In this section we also prove that the (first order) zero dynamics associated to (4.2), is "extremely slow"—with respect to the overall bandwidth of the VSR. Since this zero "attracts" one of the poles of the closed–loop system it stymies the achievement of fast transient responses. This situation motivates the inclusion of an outer–loop primary controller that generates the references to the inner–loop PI. This modification is presented in Section 6.

5.1 Zero dynamics analysis of the passive output y

Before presenting the main result of this subsection we make the important observation that the zero dynamics of the VSR model (4.7) and of its corresponding incremental version are the same. Indeed, the zero dynamics describes the behavior of the dynamical system restricted to the set where the output is zero. Since the incremental model dynamics is the *same* as the original model dynamics—simply adding and substracting a constant—their zero dynamics coincide.

Proposition 5.1 Fix $(i_d^\star, i_q^\star, v_C^\star) \in \mathcal{E}$ with $i_q^\star = 0$. The

[5] This discussion pertains only to the behavior of the adopted mathematical model of the VSR. In practice, other dynamical phenomena and unmodeled effects may trigger instability even for the PI–PBC.

zero dynamics[6] of the VSR (4.7) with respect to the output (4.13) is *exponentially stable* and is given by

$$\dot{v}_C = -\lambda v_C + \lambda v_C^\star, \tag{5.1}$$

where

$$\lambda := \frac{R(i_d^\star)^2 + G(v_C^\star)^2}{L(i_d^\star)^2 + C(v_C^\star)^2}. \tag{5.2}$$

PROOF. Setting the output (4.13) identically to zero and using the fact that $i_q^\star = 0$ we get

$$i_d = \frac{i_d^\star}{v_C^\star} v_C, \qquad i_q = \frac{i_q^\star}{v_C^\star} v_C = 0. \tag{5.3}$$

Replacing (5.3) into (4.7) gives

$$L\frac{i_d^\star}{v_C^\star}\dot{v}_C = -R\frac{i_d^\star}{v_C^\star}v_C - v_C u_1 + v_d \tag{5.4}$$

$$0 = -L\omega\frac{i_d^\star}{v_C^\star}v_C - v_C u_2 \tag{5.5}$$

$$C\dot{v}_C = \frac{i_d^\star}{v_C^\star}v_C u_1 - Gv_C - i_{dc}. \tag{5.6}$$

To eliminate u_1 we multiply (5.6) by $\frac{v_C^\star}{i_d^\star}$ and add it to (5.4) yielding

$$\left(\frac{Cv_C^\star}{i_d^\star} + \frac{Li_d^\star}{v_C^\star}\right)\dot{v}_C = -\left(\frac{Ri_d^\star}{v_C^\star} + \frac{Gv_C^\star}{i_d^\star}\right)v_C + v_d - \frac{v_C^\star}{i_d^\star}i_{dc}.$$

The proof is completed noting from (4.10) that, for $(i_d^\star, i_q^\star, v_C^\star) \in \mathcal{E}$ with $i_q^\star = 0$, we have

$$v_d - \frac{v_C^\star}{i_d^\star}i_{dc} = \frac{R(i_d^\star)^2 + G(v_C^\star)^2}{i_d^\star}$$

and pulling out the common factor $\frac{1}{i_d^\star v_C^\star}$.

Remark 5.2 The parameters R and G, that represent the losses in the VSR, are usually small—compared to L and C. Consequently, λ will also be a small value, placing the pole of the zero dynamics very close to the origin and inducing slow convergence.

Remark 5.3 It is interesting to note that the rate of exponential convergence of the zero dynamics can be rewritten

$$\lambda = \frac{1}{2}\frac{P^\star - P_{dc}^\star}{\mathcal{H}(i_d^\star, i_q^\star, v_C^\star)}$$

that is half the ratio between the steady–state dissipated power and the steady–state energy of the system. This relationship holds true also for the case $i_q^\star \neq 0$.

5.2 Zero dynamics analysis of y_I

Before analyzing the zero dynamics of the PQ and DC voltage control outputs, (4.11) and (4.12), respectively, we recall that the references do not necessarily belong to the assignable equilibrium set. However, we make the reasonable assumption that, for the chosen reference values, the zero dynamics admits an *equilibrium*—if this is not the case the zero dynamics is unstable. Moreover, similarly to the case of the passive output, we will take $i_q^{\text{ref}} = 0$.

Proposition 5.4 Fix $i_d^{\text{ref}} \in \mathbb{R}$, $i_q^{\text{ref}} = 0$. The zero dynamics of the VSR (4.7) with respect to the output (4.11) is given by

$$C\dot{v}_C = -Gv_C + \frac{\alpha_I}{v_C} - i_{dc}^{\text{ref}}, \tag{5.7}$$

where we defined the constant

$$\alpha_I := v_d i_d^{\text{ref}} - R(i_d^{\text{ref}})^2,$$

and i_{dc}^{ref} is a constant value for i_{dc} satisfying

$$(i_{dc}^{\text{ref}})^2 > 4G\alpha_I. \tag{5.8}$$

- If $\alpha_I > 0$ the zero dynamics has one equilibrium and it is *stable*.
- If $\alpha_I < 0$ the zero dynamics has two equilibria one stable and one unstable.
- If $\alpha_I = 0$ the zero dynamics is a linear asymptotically *stable* system.

PROOF. Setting the output (4.11) equal to zero with $i_q^* = 0$ and replacing into (4.7) gives

$$0 = -Ri_d^{\text{ref}} - v_C u_1 + v_d \tag{5.9}$$

$$0 = -L\omega i_d^{\text{ref}} - v_C u_2 \tag{5.10}$$

$$C\dot{v}_C = i_d^{\text{ref}} u_1 - Gv_C - i_{dc}^{\text{ref}}, \tag{5.11}$$

where we have added the superscript $(\cdot)^{\text{ref}}$ to i_{dc}. Replacing u_1 obtained from (5.9) into (5.11) yields directly (5.7). Condition (5.8) is then necessary and sufficient for the existence of a (real) equilibrium of (5.7). If $\alpha_I = 0$ the dynamics reduces to $C\dot{v}_C = -Gv_C - i_{dc}^{\text{ref}}$. The proof is completed, recalling that $v_C > 0$ and looking at the plots of the right hand side of (5.7) for the the first two cases of α_I in Fig. 3.

Remark 5.5 From Fig. 3, if $\alpha_I < 0$, it is easy to see that the stable equilibrium point is the largest one. For

[6] With some abuse of notation, the zero dynamics is represented using the same symbols of the system dynamics.

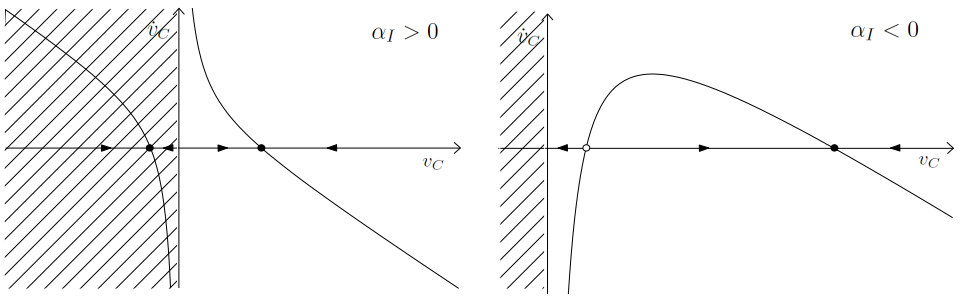

Fig. 3. Plot of $\dot{v}_C$ versus v_C for the cases of (a) $\alpha_I > 0$ and (b) $\alpha_I < 0$. The arrows in the horizontal axis indicate the direction of the flow.

standard values of the system parameters it turns out that this equilibrium is located beyond the physical operating regime of the system, hence it is of no practical interest.

Remark 5.6 Because the parameters R and G are usually very small and i_{dc}^{ref} can assume positive or negative values in standard operation. Consequently, condition (5.8) is always verified while α_I can assume positive or negative values.

5.3 Zero dynamics analysis of y_V

Proposition 5.7 Fix $v_C^{\text{ref}} \in \mathbb{R}$, $i_q^{\text{ref}} = 0$. The zero dynamics of the VSR (4.7) with respect to the output (4.12) is given by

$$L\frac{di_d}{dt} = -Ri_d - \frac{\alpha_V}{i_d} + v_d, \tag{5.12}$$

where we defined the constant

$$\alpha_V := i_{dc}^{\text{ref}} v_C^{\text{ref}} + G(v_C^{\text{ref}})^2$$

and i_{dc}^{ref} is a constant value for i_{dc} satisfying

$$v_d^2 > -4R\alpha_V. \tag{5.13}$$

- If $\alpha_V < 0$ the zero dynamics has two equilibria and they are both *stable*.
- If $\alpha_V > 0$ the zero dynamics has two equilibria one stable and one unstable.
- If $\alpha_V = 0$ the zero dynamics is a linear asymptotically *stable* system.

PROOF. Setting the output (4.12) equal to zero with $i_q^* = 0$ and replacing into (4.7) gives

$$L\frac{di_d}{dt} = -Ri_d - v_C^{\text{ref}} u_1 + v_d \tag{5.14}$$

$$0 = -L\omega i_d - v_C^{\text{ref}} u_2 \tag{5.15}$$

$$0 = i_d u_1 - G v_C^{\text{ref}} - i_{dc}. \tag{5.16}$$

Replacing u_1 obtained from (5.16) into (5.14) yields directly (5.12). Condition (5.13) is necessary and sufficient for the existence of a (real) equilibrium of (5.12). The proof is completed invoking the same arguments used in the proof of Proposition 5.4 and are omitted for brevity.

Remark 5.8 Similarly to Remark 5.6 and i_d^{ref} can assume positive or negative values in standard operation and condition (5.13) is always verified, while α_V can assume positive or negative values.

5.4 Simulated evidence of the performance limitations

Although Proposition 5.1 proves that the zero dynamics for the passive output y is exponentially stable it turns out that, for the components used in standard HVDC transmission system, the convergence rate is $\lambda \approx 0.04$, which is extremely slow. As indicated above this dominating dynamics stymies the achievement of fast transient responses—situation that is shown in the following simulations. Also, we present simulated evidence of unstable behavior of PI inner–loops using the outputs (4.11) and (4.12).
We consider a three–terminals HVDC transmission system with a simple *meshed* topology, that is illustrated in Fig. 4, where the corresponding graph is also given. The model of the system is given by (2.9), that is a system of dimension $3n + \ell = 11$ with $2n = 6$ inputs. Parameters of the VSRs and of the transmission lines are given in Table 1.

We define the following *control objectives*: all the stations are required to regulate the reactive power to zero;

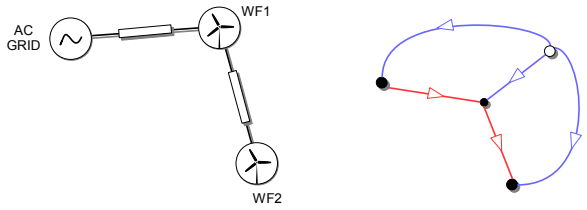

Fig. 4. Schematic representation of an HVDC transmission system constituted by three stations, associated to two wind farms (WFs) and an AC grid, with associated graph. The graph is represented by filled circles for the *VSRs-buses* and the unfilled circle for the *ground* node. Blue and red edges characterize VSRs and lines, respectively.

Parameter	Value	Parameter	Value
$R_{r,i}$	$0.01\ \Omega$	$G_{r,i}$	$0\ \Omega^{-1}$
$L_{r,i}$	$40\ mH$	$C_{r,i}$	$20\ \mu F$
V_i	$130\ kV$	ω_i	$50\ Hz$
$R_{\ell,12}$	$26\ \Omega$	$L_{\ell,12}$	$3.76\ mH$
$R_{\ell,23}$	$20\ \Omega$	$L_{\ell,23}$	$2.54\ mH$

Table 1
Three stations HVDC transmission system parameters.

the stations associated to the wind farms (WF1, WF2) are required to regulate the active power to desired (constant) values; the remaining station, called *slack bus* (SB), must regulate the voltage around its nominal value. In Table 2, the corresponding references of direct current and DC voltages are furnished, together with the corresponding assignable equilibria, that are calculated via the PFSSE defined by (3.3). Changes in references occur every T s over a time interval of $5T$ s. It should be noticed that from 0 to $2T$ the power flow is uniquely directed from both wind farms stations to the AC grid, while at $2T$, and next $3T$ the wind farms stations start demanding power to the AC grid, thus reversing the direction of the power flow. This situation can arise when the power produced by the wind farms is insufficient to supply local loads.

5.4.1 PI–PBC

In this subsection we present simulations on the three–terminals benchmark example of the decentralized PI–PBC defined in Subsection 4.2, which illustrate the stability properties and performance limitations discussed in the previous sections. Setting $T = 2000$ s the controllers (4.5) are designed with identical parameters and diagonal matrices $k_{P,i} = \text{diag}\{1, 1\}$, $k_{I,i} = \text{diag}\{10, 10\}$. The behavior of the VSRs are depicted in Fig. 5.

	$\mathbf{i_d^\star(A)}$			$\mathbf{v_C^\star(kV)}$		
	SB	WF_1	WF_2	SB	WF_1	WF_2
0	-1260	900	1000	100	142.595	158.951
T	-1588	900	1800	100	153.650	179.691
$2T$	-266	500	-200	100	109.004	104.004
$3T$	905	-400	-200	100	69.419	60.877
$4T$	-849	1300	-200	100	128.708	124.532

Table 2
Three stations HVDC transmission system references from 0 to $5T$.

As expected, the direct currents of each station attain the assignable equilibria defined in Table 2, while the quadrature currents are always kept to zero after a very short transient. Moreover, the DC voltage at the slack bus is maintained near the nominal value of 100 kV, as required, while the DC voltage variation at the wind farms stations, balances the fluctuation of power demand. Even though the desired steady–state is attained, for all practical purposes, the convergence time of direct currents and DC voltages is extremely slow. This poor transient performance behavior is independent of the controller gains. Indeed, extensive simulations show that the system maintains the same slow convergence time even with larger gains, thus validating the performance limitations analysis realized in subsection 5.1.

5.4.2 PQ and DC voltage controllers

We next analyze the behavior of the system under the standard PQ and DC voltage controllers of Subsection 4.3. In agreement with the control requirements described above, two PQ controllers are designed to regulate direct and quadrature currents of the wind farms stations, and one DC voltage controller is designed to regulate DC voltage and quadrature current of the slack bus. We consider simple PI controllers defined over the outputs (4.11), (4.12), designed with identical gains $k_{P,i}$, $k_{I,i}$, that are tuned via simulations. The behavior of the VSRs are depicted in Fig. 6, with $T = 4$ s. This value should be contrasted with the value ($T = 2000$ s) used for the PI–PBC. It is easy to see that the PQ and DC voltage controllers correctly (and rapidly) regulate the station at the desired references between 0 and 8 s. This good behavior is not surprising, because PQ controllers applied to VSRs that are injecting power and a DC voltage controller applied to VSRs that is absorbing power, have associated globally asymptotically stable zero dynamics, as proved in Subsections 5.2, 5.3. On the other hand,as shown in the figures, when at stations $WF1$ and $WF2$ the power flow is reversed (respectively at $t = 12$ s and $t = 8$ s), the correspondent DC voltages go unstable, because in these cases the zero dynamics is unstable. Similar unstable behavior appears also at the slack bus station.

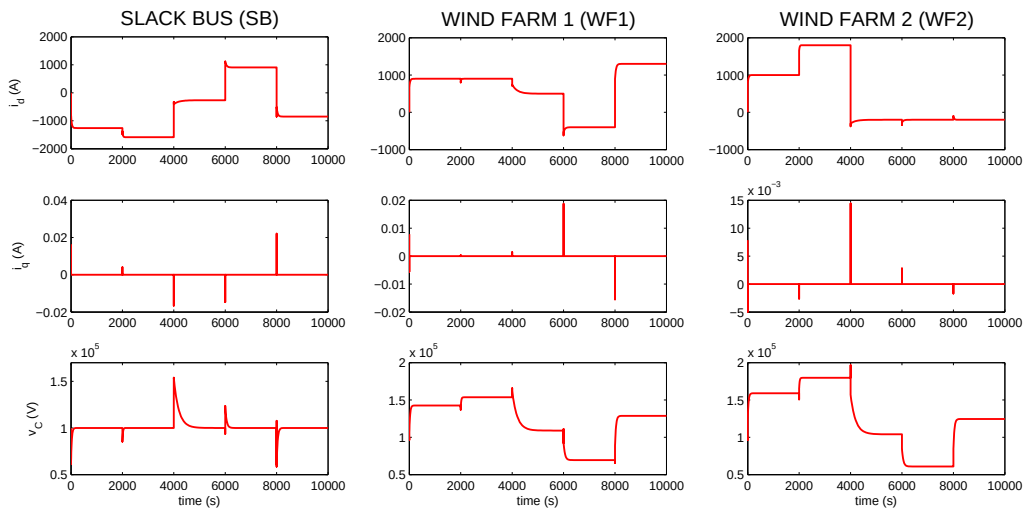

Fig. 5. Responses of VSRs variables under the decentralized PI–PBC.

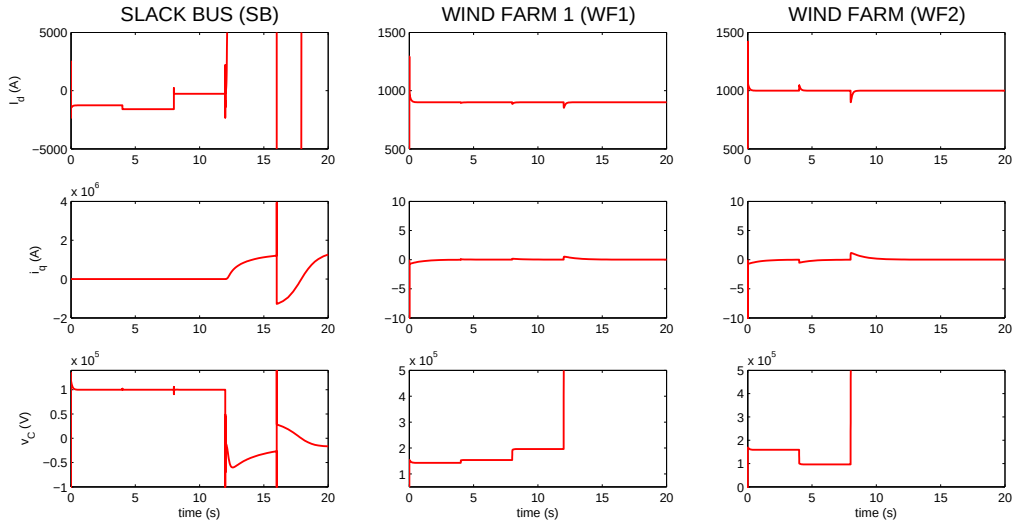

Fig. 6. Responses of VSRs variables under the decentralized PQ and DC voltage controllers.

6 Adding a Primary Control to the PI–PBC

To overcome the transient performance limitations of the PI–PBC exhibited in Subsection 5.4.1 we propose in this section to add to it an outer–loop—known in power systems literature as *primary control*. The task of this control is to generate the references to the inner–loop scheme that replace the desired equilibria in the definition of the passive output (4.13).

6.1 New output with droop control

A commonly used primary control is the so–called *droop control*, which replaces $i_d^\star$ with the desired reference i_d^{ref} plus a deviation (droop) term proportional to the voltage error, leaving some constant references for $i_q^\star$ and $v_C^\star$—see Fig. 7. More precisely, the following assignments are made in (4.13)

$$i_d^\star \leftarrow i_d^{\text{ref}} + K_d(v_C^{\text{ref}} - v_C), \quad i_q^\star \leftarrow i_q^{\text{ref}}, \quad v_C^\star \leftarrow v_C^{\text{ref}}, \tag{6.1}$$

where $K_d > 0$ is called the droop coefficient and, as done before, we have used the notation $(\cdot)^{\text{ref}}$ to underscore that these values do not necessarily belong to the assignable set. Replacing (6.1) in the passive output (4.13) yields the new output

$$y_N := \begin{bmatrix} v_C^{\text{ref}} i_d - i_d^{\text{ref}} v_C - K_d(v_C^{\text{ref}} - v_C)v_C \\ v_C^{\text{ref}} i_q - i_q^{\text{ref}} v_C \end{bmatrix}. \tag{6.2}$$

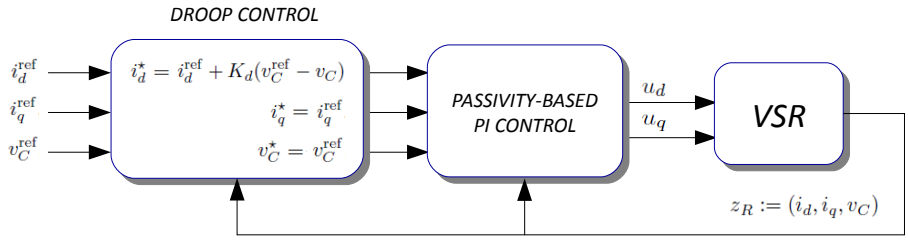

Fig. 7. Closed–loop representation of the inner–loop PI–PBC plus the primary droop controller.

6.2 Stability analysis

The performance of the modified PI–PBC, that is, adding a PI around the new outputs (6.2) is significantly better than the original PI–PBC as shown in the simulations given below. However, it is evident from (6.2) that the inclusion of additional state–dependent terms to the first component of y_N, as well as the fact that the reference signals do not belong to $\mathcal{E}$, invalidates the stability result obtained in Proposition 4.2, as the new output y_N is not passive anymore.

Consequently, to guarantee the correct behavior of the VSR a new proof of stability is required. To establish this result we assume that inner–loop PI and the VSRs are much faster than the network dynamics. Under this assumption we can model the AC side of the VSR as the parallel interconnection of two AC current sources connected to the network through a voltage bus capacitor, that is assumed to operate at the same time–scale of the network, see Fig. 8.

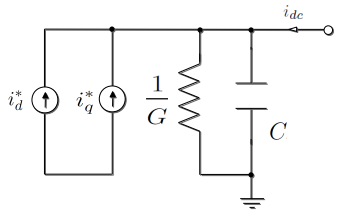

Fig. 8. VSR modeled as ideal current sources connected to a voltage bus capacitor, in dq–frame.

By simple application of Kirchhoff's currents law to Fig. 8 it is possible to write the scalar differential equation

$$\begin{aligned}\dot{q}_C &= -\frac{G}{C}q_C + i_d^\star + i_q^\star - i_{dc} = \\ &= -\left[\frac{G+K_d}{C}\right]q_C + i_d^{\rm ref} + \frac{K_d}{C}q_C^{\rm ref} + i_q^{\rm ref} - i_{dc},\end{aligned}$$

where we have used (6.1) and the definition $q_C^{\rm ref} := Cv_C^{\rm ref}$ to get the second identity. This can be rewritten in a more compact form

$$\dot{q}_C = -\left[\frac{G+K_d}{C}\right]q_C + i_{ac} - i_{dc}, \tag{6.3}$$

with $i_{ac} := i_d^{\rm ref} + \frac{K_d}{C}q_C^{\rm ref} + i_q^{\rm ref}$. In order to obtain the interconnected model of the closed–loop system (with meshed topology) we follow the same modeling procedure of Section 2, replacing the full model of the VSRs given by (2.2) with n scalar equations of the form (6.3). The set of n scalar droop–controlled VSRs can be written in pH form

$$\begin{aligned}\dot{x}_C &= -\mathcal{R}_C\nabla\mathcal{H}_C + I - i_C \\ v_C &= \nabla\mathcal{H}_C\end{aligned} \tag{6.4}$$

with the following definitions.

- State space vector the collection of capacitor charges of each VSR, that is, $x_C := \text{col}(q_{C,i})$.
- Energy function $\mathcal{H}_C(x_C) := \frac{1}{2}x_C^\top Q_C x_C$, with $Q_C := \text{diag}\{\frac{1}{C_i}\}$.
- External source $I := \text{col}(i_{ac,i}) \in \mathbb{R}^n$, with $i_{ac,i}$ defined in (6.3) that, following (6.3) we decompose into

$$I = I_D^{\rm ref} + I_Q^{\rm ref} + K_D Q_C x_C^{\rm ref},$$

  where $I_D^{\rm ref} = \text{col}(i_{d,i}^{\rm ref})$, $I_Q^{\rm ref} = \text{col}(i_{q,i}^{\rm ref})$, $x_C^{\rm ref} = \text{col}(q_{C,i}^{\rm ref})$
- Port variables the out–going currents $i_C = \text{col}(i_{dc,i}) \in \mathbb{R}^n$ and the DC voltages $v_C = \text{col}(v_{dc,i}) \in \mathbb{R}^n$.
- Dissipation matrix

$$\mathcal{R}_C := R_G + K_D \tag{6.5}$$

  where $R_G := \text{diag}\{G_i\}$ and $K_D := \text{diag}\{K_{d,i}\}$.

Combining (6.4) with the pH representation of the lines (2.5) via the power preserving interconnection laws of

Subsection 2.4 we obtain the following global pH system

$$\dot{x} = (\mathcal{J} - \mathcal{R})\nabla\mathcal{H} + gI, \tag{6.6}$$

with the following definitions.

- State space vector $x = \text{col}(x_C, x_L) \in \mathbb{R}^{n+\ell}$.
- Energy function $\mathcal{H}(x) := \mathcal{H}_C(x_C) + \mathcal{H}_L(x_L) = \frac{1}{2}x^\top Q x$, with $Q := \text{bdiag}\{Q_C, Q_L\}$.
- Interconnection and dissipation matrices $\mathcal{J}, \mathcal{R} \in \mathbb{R}^{n+\ell}$ and input matrix $g \in \mathbb{R}^{(n+\ell)\times n}$

$$\mathcal{J} := \begin{bmatrix} 0_n & -M_1 \\ M_1^\top & 0_\ell \end{bmatrix}, \quad \mathcal{R} := \begin{bmatrix} \mathcal{R}_C & 0_{n\times\ell} \\ 0_{n\times\ell}^\top & \mathcal{R}_L \end{bmatrix}, \quad g := \begin{bmatrix} \mathbb{I}_n \\ 0_{\ell\times n} \end{bmatrix}.$$

The first observation we make is that the droop–controlled HVDC transmission system with meshed topology (6.6) is a linear time invariant system of the form $\dot{x} = Ax + gI$, where $A := (\mathcal{J} - \mathcal{R})Q$. Second, it is easy to show that A is a Hurwitz matrix with strict Lyapunov function $x^\top Q x$. Consequently, all trajectories converge to the equilibrium $x^\star = A^{-1}gI$. In the light of these observations, the proposition below follows immediately.

Proposition 6.1 *The equilibrium $x^\star$ of the system* (6.6) *is globally exponentially stable. Moreover, if*

$$-R_G Q_C x_C^{\text{ref}} - M_1 \mathcal{R}_L^{-1} M_1^\top Q_C x_C^{\text{ref}} + I_D^{\text{ref}} + I_Q^{\text{ref}} = 0, \tag{6.7}$$

the coordinates x_C converge to x_C^{ref}.

Remark 6.2 From (6.5) it is clear that the droop coefficients $K_{d,i}$ inject additional dissipation into the voltage dynamics—speeding up the convergence rate. Without droop control the convergence is very slow due to the small value of the VSR conductances G_i.

Remark 6.3 In contrast to [3], the droop control laws are defined with respect to a set of voltage references verifying (6.7), that obviously do not all coincide with the nominal voltage. In this way, the trade–off between having the voltages converge to the nominal voltage, and satisfying a pre–determined active power distribution (*sharing*) between the VSRs, is completely captured by condition (6.7), that is independent from droop coefficients.

6.3 Simulations

To illustrate the discussion above about primary control, we consider again the three–terminal benchmark example described in Subsection 5.4, controlled via decentralized PI–PBC. We employ the same controllers parameters of Subsection 5.4.1, and further analyze the benefits in terms of performances, provided by adding a droop control stage to the PI–PBC controllers. For the choice of the droop coefficients we propose a very simple heuristics, based on Remark 6.2. Because droop coefficients are supposed to quantify the additional dissipation injected into the voltage dynamics, and because the rate of convergence of the same depend from the value of the capacitances, define

$$d_i = \frac{G_i + K_{d,i}}{C_i} \tag{6.8}$$

as a measure of the convergence rate of the i-th station, with G_i and $K_{d,i}$ the conductance and the droop coefficient of the VSR, respectively. A possible choice of droop coefficients is to a define a common convergence rate d such that $d_i = d$ for every i, that is equivalent to define an uniform convergence rate over the three stations. In the three–terminal benchmark example, because parameters are supposed to be identical at each VSR, the droop coefficients $K_{d,i} = 5 \cdot 10^{-3}$ will take identical values.

The behavior of the VSRs are then given in Fig. 9. Differently from subsection 5.4.1 the references changes occur every $T = 2$ s. It is easy to see that, compared to Fig. 5, the responses maintain the same shape while the convergence occur with a rate $\approx 10^3$ faster.

7 Secondary Control

In this section we provide a reformulation of the problem of choosing appropriate references for the primary (droop) or inner PI controllers presented in the previous sections. In power system literature this is often referred as *secondary control* and it is in general characterized by a centralized or distributed architecture. In particular we show how certain secondary control strategies—widely used in power system literature—can be mathematically formalized using the PFSSE.

In order to provide a formal formulation of the mentioned problem, we consider an HVDC transmission system with *meshed* topology composed by n VSRs (stations), and described by the pH system (2.9). The set of assignable references is determined by the following PFSSE

$$\begin{aligned} &-R_i(i_{d,i}^{\text{ref}})^2 - R_i(i_{q,i}^{\text{ref}})^2 - G_i(v_{C,i}^{\text{ref}})^2 + \\ &\quad + v_{d,i} i_{d,i}^{\text{ref}} - v_{C,i}^{\text{ref}} M_{1,i} \mathcal{R}_L^{-1} M_{1,i}^\top v_C^{\text{ref}} = 0, \end{aligned} \tag{7.1}$$

for $i \in [1, n]$, where the row vector $M_{1,i} \in \mathbb{R}^n$ is the i–th row of the matrix M_1, that coincide with (3.2), but in co-energy variables. The PFSSE consist in n quadratic, coupled equations in $3n$ variables, one for each station. A possibility is then to directly assign $2n$ variables, that correspond to the desired references, while the remaining n can be easily determined via (7.1) and then pro-

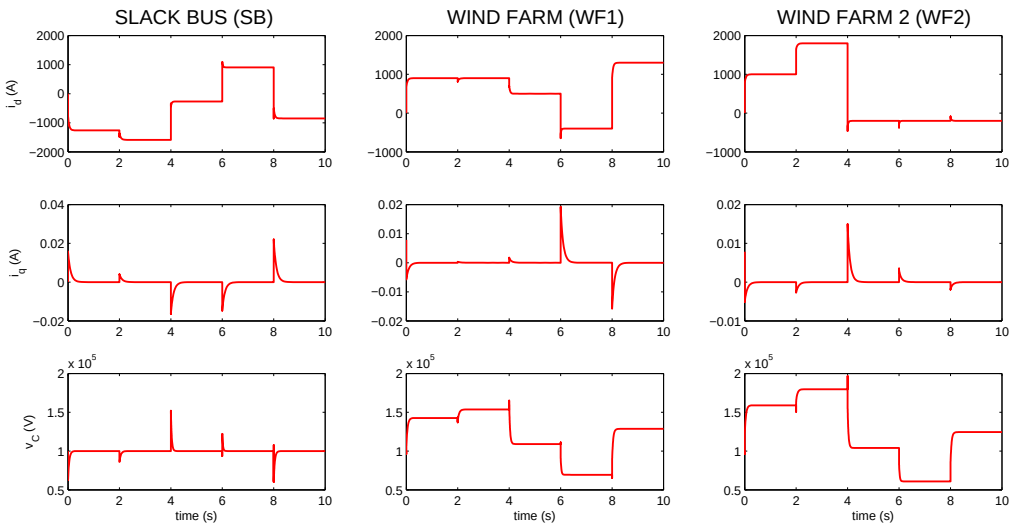

Fig. 9. Responses of VSRs variables with the decentralized PI–PBC plus droop control.

vided to the inner controllers. However, the choice of which variables have to be chosen as desired references is not arbitrary, but depends on the control objectives to satisfy. We next illustrate how the problem of defining references in conformity with some natural control objectives is formalized using the PFSSE.
Consider the following requirements for the n stations: keep the DC voltage of only one station (called *slack bus*) near to the nominal value, guarantee a proportional active power distribution (*power sharing*) among the stations, regulate the reactive power to a desired value at each station. These requirements can be easily reformulated as constraints over the PFSSE as follows:

- regulation of the DC voltage of the *slack bus*

$$v_{C,n}^{\text{ref}} = v_{C,n}^{\text{d}},$$

  where $v_{C,n}^{\text{d}}$ represents the DC voltage nominal value;
- proportional *power sharing*

$$P_i^{\text{ref}} = \alpha_i P_n^{\text{ref}} \quad \Rightarrow \quad i_{d,i}^{\text{ref}} = \alpha_i i_{d,n}^{\text{ref}}, \qquad i \in [1, n-1]$$

  where α_i is a ratio that determines the proportional active power distribution of the i-th station with respect to the *slack bus*;
- regulation of the reactive power

$$Q_i^{\text{ref}} = Q_i^{\text{d}} \quad \Rightarrow \quad i_{q,i}^{\text{ref}} = i_{q,i}^{\text{d}}, \qquad i \in [1, n]$$

  where Q_i^{d} represents the exact reactive power required to be injected (or absorbed) by the i-th station.

It is easy to see that the equations above constitute indeed a set of $2n$ assignments for the PFSSE, that can be consequently solved with respect to the remaining variables.

8 Conclusions and future perspectives

The work covers different aspects of modeling, analysis and control of multi–terminal HVDC transmission system. The main contribution is a decentralized, globally asymptotically stable, PI control for a very general class of multi–terminal HVDC transmission systems. For this purpose, starting from a graph description of the network, a pH representation has been obtained, thus revealing the intrinsic passivity properties of the system. The main result is a direct extension of the previous works on PI control of VSRs, to a sufficiently general interconnected system, with the important property that the control is decentralized, a fundamental requirement for large–scale systems.

To provide some connections between the proposed controller and standard techniques, widely used in literature, a comparative analysis of stability and performances is provided, shedding some light on limitations and benefits of different approaches. In particular it is proved—and validated via simulations—that the popular current and voltage control techniques possibly lead to unstable behaviors of the controlled system, while the proposed PI–PBC, although ensuring convergence, has clear performance limitations. The theoretical explanation of these performances results from a detailed zero dynamics analysis. To overcome the performance limitations of the PI–PBC we follow the standard practice of adding an outer controller. Under a practically reasonable time–scaling assumption, a formal stability proof of the modified PI–PBC is provided. Some brief

discussion on a possible formalization of secondary control is also given.

A more accurate description of the system, that may improve the control quality, is obtained representing the lines by means of the Telegrapher's equations, thus leading to an infinite dimensional pH representation, which can still be handled with existing theory [37]. From a more practical viewpoint, it would be also of great interest to reformulate standard strategies in secondary control, moving from the PFSSE. A viable possibility is to consider the latter as a problem of static optimization, with respect to which the control requirements can be elegantly formalized.

Acknowledgements

This work was supported by the Ministry of Education and Science of Russian Federation (Project 14.Z50.31.0031).

References

[1] A.M. Abbas and P.W. Lehn. PWM based VSC-HVDC systems – a review. In *Power Energy Society General Meeting, 2009. PES '09. IEEE*, pages 1–9, July 2009.

[2] H. Akagi. *Instantaneous Power Theory and Applications to Power Conditioning*. Wiley, Newark, 2007.

[3] M. Andreasson, M. Nazari, D. V. Dimarogonas, H. Sandberg, K. H. Johansson, and M. Ghandhari. Distributed Voltage and Current Control of Multi-Terminal High-Voltage Direct Current Transmission Systems. *ArXiv e-prints*, November 2013.

[4] M.K. Bucher, R. Wiget, G. Andersson, and C.M. Franck. Multiterminal HVDC Networks – what is the preferred topology? *Power Delivery, IEEE Transactions on*, 29(1):406–413, Feb 2014.

[5] C.I. Byrnes, A. Isidori, and J.C. Willems. Passivity, feedback equivalence, and the global stabilization of minimum phase nonlinear systems. *Automatic Control, IEEE Transactions on*, 36(11):1228–1240, Nov 1991.

[6] J.M. Carrasco, L.G. Franquelo, J.T. Bialasiewicz, E. Galvan, R.C.P. Guisado, Ma.A.M. Prats, J.I. Leon, and N. Moreno-Alfonso. Power-electronic systems for the grid integration of renewable energy sources: A survey. *Industrial Electronics, IEEE Transactions on*, 53(4):1002–1016, June 2006.

[7] S. Chatzivasileiadis, D. Ernst, and G. Andersson. The global grid. *CoRR*, abs/1207.4096, 2012.

[8] H. Chen, Z. Xu, and F. Zhang. Nonlinear control for VSC based HVDC system. In *Power Engineering Society General Meeting, 2006. IEEE*, pages 5 pp.–, 2006.

[9] Y. Chen, J. Dai, G. Damm, and F. Lamnabhi-Lagarrigue. Nonlinear control design for a multi-terminal VSC-HVDC system. In *Control Conference (ECC), 2013 European*, pages 3536–3541, July 2013.

[10] G. Escobar, A.J. Van Der Schaft, and R. Ortega. A Hamiltonian viewpoint in the modeling of switching power converters. *Automatica*, 35(3):445–452, March 1999.

[11] S. Fiaz, D. Zonetti, R. Ortega, J.M.A. Scherpen, and A.J. van der Schaft. A port-Hamiltonian approach to power network modeling and analysis. *European Journal of Control*, 19(6):477 – 485, 2013. Lagrangian and Hamiltonian Methods for Modelling and Control.

[12] N. Flourentzou, V.G. Agelidis, and G.D. Demetriades. VSC-based HVDC power transmission systems: An overview. *Power Electronics, IEEE Transactions on*, 24(3):592–602, Mar 2009.

[13] B.A. Francis and G. Zames. On H^∞-optimal sensitivity theory for siso feedback systems. *Automatic Control, IEEE Transactions on*, 29(1):9–16, Jan 1984.

[14] O. Gomis-Bellmunt, J. Liang, J. Ekanayake, R. King, and N. Jenkins. Topologies of multiterminal HVDC-VSC transmission for large offshore wind farms. *Electric Power Systems Research*, 81(2):271 – 281, 2011.

[15] T.M. Haileselassie, T. Undeland, and K. Uhlen. Multiterminal HVDC for offshore windfarms control strategy. European Power Electronics and Drives Association, 2009.

[16] M. Hernandez-Gomez, R. Ortega, F. Lamnabhi-Lagarrigue, and G. Escobar. Adaptive PI stabilization of switched power converters. *Control Systems Technology, IEEE Transactions on*, 18(3):688–698, 2010.

[17] A. Isidori. *Nonlinear Control Systems*. Springer-Verlag New York, Inc., Secaucus, NJ, USA, 3rd edition, 1995.

[18] A. Jager-Waldau. Photovoltaics and renewable energies in europe. *Renewable and Sustainable Energy Reviews*, 11(7):1414 – 1437, 2007.

[19] B. Jayawardhana, R. Ortega, E. Garcia-Canseco, and F. F. Castaños. Passivity of nonlinear incremental systems: Application to PI stabilization of nonlinear RLC circuits. In *Decision and Control, 2006 45th IEEE Conference on*, pages 3808–3812, 2006.

[20] S.G. Johansson, G. Asplund, E. Jansson, and R. Rudervall. Power system stability benefits with VSC DC-transmission systems. In *CIGRE Conference, Paris, France*, 2004.

[21] M.P. Kazmierkowski, R. Krishnan, F. Blaabjerg, and J.D. Irwin. *Control in Power Electronics: Selected Problems*. Academic Press Series in Engineering. Elsevier Science, 2002.

[22] NM Kirby, MJ Luckett, L Xu, and Werner Siepmann. HVDC transmission for large offshore windfarms. In *AC-DC Power Transmission, 2001. Seventh International Conference on (Conf. Publ. No. 485)*, pages 162–168. IET, 2001.

[23] T. Lee. Input-output linearization and zero-dynamics control of three-phase AC/DC voltage-source converters. *Power Electronics, IEEE Transactions on*, 18(1):11–22, Jan 2003.

[24] H. Lund. Large-scale integration of wind power into different energy systems. *Energy*, 30(13):2402–2412, 2005.

[25] M. Perez, R. Ortega, and J.R. Espinoza. Passivity-based PI control of switched power converters. *Control Systems Technology, IEEE Transactions on*, 12(6):881–890, 2004.

[26] R.T. Pinto, S.F. Rodrigues, P. Bauer, and J. Pierik. Comparison of direct voltage control methods of multi-terminal dc (MTDC) networks through modular dynamic models. In *Power Electronics and Applications (EPE 2011), Proceedings of the 2011-14th European Conference on*, pages 1–10, Aug 2011.

[27] L. Qiu and E. J. Davison. Performance limitations of non-minimum phase systems in the servomechanism problem. pages 337–349, 1993.

[28] S. Sanchez, R. Ortega, R. Gri no, G. Bergna, and M. Molinas-Cabrera. Conditions for existence of equilibrium points of

systems with constant power loads. In *Decision and Control, 2013 52nd IEEE Conference on, Firenze, Italy*, 2013.

[29] S.R. Sanders and G.C. Verghese. Lyapunov-based control for switched power converters. *Power Electronics, IEEE Transactions on*, 7(1):17–24, Jan 1992.

[30] M.M. Seron, J.H. Braslavsky, and G.C. Goodwin. *Fundamental Limitations in Filtering and Control*. Springer Publishing Company, Incorporated, 1st edition, 2011.

[31] S. Shah, R. Hassan, and J. Sun. HVDC transmission system architectures and control - a review. In *Control and Modeling for Power Electronics (COMPEL), 2013 IEEE 14th Workshop on*, pages 1–8, June 2013.

[32] D. Shuai and X. Zhang. Input-output linearization and stabilization analysis of internal dynamics of three-phase AC/DC voltage-source converters. In *Electrical Machines and Systems (ICEMS), 2010 International Conference on*, pages 329–333, Oct 2010.

[33] J.-L. Thomas, S. Poullain, and A. Benchaib. Analysis of a robust DC-bus voltage control system for a VSC transmission scheme. In *AC-DC Power Transmission, 2001. Seventh International Conference on (Conf. Publ. No. 485)*, pages 119–124, Nov 2001.

[34] M.A. Torres. Estudio de un sistema VSC-HVDC y aplicación de método de control basado en pasividad. Master's thesis, Universidad de Concepción, Chile, March 2007.

[35] A.J. van der Schaft. *$\mathcal{L}_2$-gain and passivity techniques in nonlinear control*. Communications and control engineering. Springer, Berlin, 2000.

[36] A.J. van der Schaft. Characterization and partial synthesis of the behavior of resistive circuits at their terminals. *Systems and Control Letters*, 59(7):423 – 428, 2010.

[37] A.J. van der Schaft and D. Jeltsema. *Port-Hamiltonian Systems Theory: An Introductory Overview*. now publishers Inc, 2014.

[38] A. Yazdani and R. Iravani. *Voltage–Sourced Controlled Power Converters – Modeling, Control and Applications*. Wiley IEEE, 2010.

[39] D. Zonetti. A port–Hamiltonian approach to power systems modeling. Master's thesis, Université de Paris-Sud XI, June 2011.

[40] D. Zonetti, R. Ortega, and A. Benchaib. A globally asymptotically stable dencentralized PI controller for multi–terminal high–voltage DC transmission systems. In *Proceedings of the 13th European Control Conference on*, Jun 2014.